RESEARCH ARTICLE

WILEY

Effects of characteristic parameters of isolation system on seismic response of isolated nuclear power plants

Liuyun Xu | Jinyi Zhao | Zhiguang Zhou [ID]

Department of Disaster Mitigation for Structures, Tongji University, Shanghai 200092, China

Correspondence
Zhiguang Zhou, Department of Disaster Mitigation for Structures, Tongji University, Shanghai 200092, China.
Email: zgzhou@tongji.edu.cn

Summary

Seismic isolation is increasingly being used in both traditional and industrial structures for its ability to reduce structural responses while effectively protecting systems and components, such as machinery. After applying isolation, the standardize design can be achieved during seismic design of nuclear power plant. However, the seismic response of nuclear structure with different isolation characteristic parameters under different ground motions has not been fully studied. In this paper, a new generation passive nuclear power plant model was simulated with finite element method. The acceleration response, deformation, seismic mitigation efficiency, and response discreteness of nuclear structures with different isolation characteristic parameters were analyzed. The effect degree of isolation characteristic parameters on seismic response of nuclear structures was investigated. Performance spaces are introduced as an alternate method for evaluating responses of nuclear structures. The results show that isolation systems largely reduce both the mean value and discreteness of seismic response of nuclear structures.

KEYWORDS

base isolation, floor response spectra, isolation characteristic parameters, nuclear power plant, performance spaces

1 | INTRODUCTION

Seismic or base isolation has been proven to be a revolutionary passive control technique enhancing the seismic safety of building structures. Four nuclear structures have been operated up to now with seismic or base isolation, which are Koeberg nuclear power plant (NPP), Cruas NPP, Jules Horowitz Reactor, and International Thermonuclear Experimental Reactor[1,2]. Lead-rubber bearings (LRBs), low-damping rubber bearings, and friction pendulum system are examples of isolation bearings implemented in isolated NPPs variously. Whittaker[3] described the performance expectations identified in the NUREG and ASCE 4 for seismic isolation systems, superstructures, and substructures. However, effects of characteristic parameters of isolation system on seismic response of isolated NPPs have not been studied adequately. Fan and Ahmadi[4] researched on numerical results for the seismic response of secondary systems in a three-story base-isolated structure. Khechfe et al.[5] carried on an experimental study of a base-isolated secondary system that is installed on a fixed-base three-story frame. Zhang[6] found that the elastic stiffness of isolation devices is not sensitive in affecting the damage potential when it is among the range of 0.4–1.2 times of column's elastic stiffness, preferably in a close neighborhood of the column stiffness by generating fragility curves of highway bridges. Jenna[7] studied effects of isolator models on the floor response spectra at key locations in an NPP, using time history analysis in OpenSees. Amin[8] modeled the design of base-isolated reinforced concrete building structure with Eurocode (EC8) seismic design guidelines, considering earthquake effect due to the reinforced concrete structure, and finally found that base-isolated structures shown drastic increased in story drift at the ground story but reduced significantly up to roof level. Charmpis[9,10] used genetic algorithm method to detect the isolation

configuration that minimizes the maximum floor acceleration of the building. Kelly and Tsai[11,12] carried on a series of earthquake simulator tests of a five-story steel frame to identify the impact of rubber-bearing isolation systems on seismic response of light secondary equipment. In addition, probabilistic seismic risk analysis of the base-isolated NPP was conducted under selected recorded ground motions of the Tohoku event[13], and the results show that the failure probability of NPP reactor building is much larger for long-period seismic motions. For practical design, robust design optimization method[14] was performed by optimizing the weighted sum of expected value of maximum root mean square acceleration of the superstructure as well as its dispersion. Results show that robust design optimization method yields a better performance for the system based on the upper bound solution.

Some isolation optimized results have been proposed based on the optimization methods mentioned above. Friction pendulum system exists a particular value of friction coefficient, which can minimize the top floor acceleration of multistory buildings [15] using extensive computation rather than optimization algorithm. Providakis[16] illustrated that the supplemental viscous damping provides different results between near-fault and far-fault seismic excitation for LRB-isolated structure as well as increased drifts on superstructures subjected to far-fault earthquake ground motions. Sun[17] focused on the random response and dynamic reliability with different isolator parameters (effective stiffness and effective damping ratio) and demonstrated the effect of isolator parameters on superstructure response. Kumar[18] investigated the effects of intra-earthquake changes in mechanical properties on the response of base-isolated NPPs, using an advanced numerical model of a lead-rubber bearing, and further conducted a series of experiments to validate a phenomenological model of an elastomeric bearing in tension. Huang et al [19,20] studied isolated NPPs with three type of bearings: friction pendulum systems, lead-rubber bearings, and low-damping rubber bearings, using intensity-, scenario-, and time-based assessments to compute probability and annual frequency of unacceptable performance of an NPP for a given seismic hazard. Keikha[21] assessed and numerically implemented analytical models for the newly introduced friction pendulum isolator that can identically capture its real experimental performance and also have the ability to capture the bidirectional, tridirectional, and vertical–horizontal coupling behavior of it, raising the predictive capability of nonlinear response history analyses and also lowering computational and experimental complexity and cost. Considering the relationship between floor acceleration and interstory drift ratio, Whittaker [22] introduced performance space of superstructure in which the two variables were independent and obey lognormal distribution separately. Based on this study, Huang[23] developed a performance space with a joint probability function. Moreover, AP1000 inputs for 2D SASSI analyses have been conducted by Westinghouse [24].

This paper focuses on the new generation of passive NPPs AP1000. An isolated three-stick model was set up to evaluate isolation effects. The purpose is to study seismic response and dispersion when changing key parameters of isolators. Then, the conception of performance space with two parameters was proposed to gain a comprehensive understanding of seismic response, helping avoid unnecessary trial calculations. Finally, an envelope curve of performance space was introduced to illustrate the probability boundary of isolated AP1000.

2 | MODELING OF AP1000

2.1 | AP1000 stick model

A new generation passive NPP, AP1000, is taken as the prototype for analysis and evaluation. Three major parts of AP1000 are included: auxiliary and shield building (ASB), steel containment vessel (SCV), and containment internal structures (CIS). In order to illustrate the dynamic property and the seismic response of the NPP, a finite element mass model with three sticks was built in ABAQUS to perform the response history analysis.

To describe it clearly, three internal sticks (ASB, SCV, and CIS) are horizontally separate, which are concentric and structurally independent. The discrete masses marked with pointed numbers were connected through elastic beams. Additionally, as illustrated in Figure 1, node pair 965-982 is coupled in two horizontal directions to simulate in-plane connection, and node pairs 980-962, 981-963, and 989-965 are coupled in 6° with multipoint constraint beams to simulate a complete rigid connection. The bottom elevations of ASB, SCV, and CIS sticks are 18.44, 30.48, and 18.44 m in proper order, and their total heights are 83.10, 55.44, and 33.07 m, respectively. The total mass of AP1000 are 1.532×10^5 ton. The mass ratio of ASB, SCV, and CIS in the whole model are 86, 3, and 11%, respectively. In the study of acceleration responses, the top points named 978, 1004, and 988 in ASB, SCV, and CIS sticks, respectively, are considered.

2.2 | Isolator parameters

Totally 273 LRBs are set in the isolation plane and modeled by "connector" element in ABAQUS. The layout of the isolators is shown in Figure 2, and yellow points in the figure represent LRBs. Herein, bilinear mechanical model is applied to analysis of isolation bearings. Figure 3 describes the definition of post-yield stiffness (K_2), yield strength (Q_d), and initial stiffness (K_1), which are initially 4,828.43 kN/m, 195.26 kN, and 48,284.30 kN/m, respectively. Frequency comparison of non-isolated and isolated AP1000 model is shown in Table 1.

The impact of K_2, Q_d, and K_1 on response of base-isolated AP1000 model is studied. To investigate a wide range of isolation bearing properties, the three parameters change from 50 to 150% of their initial value, adapting 25% as a step size. Figure 4 shows force-displacement curves of
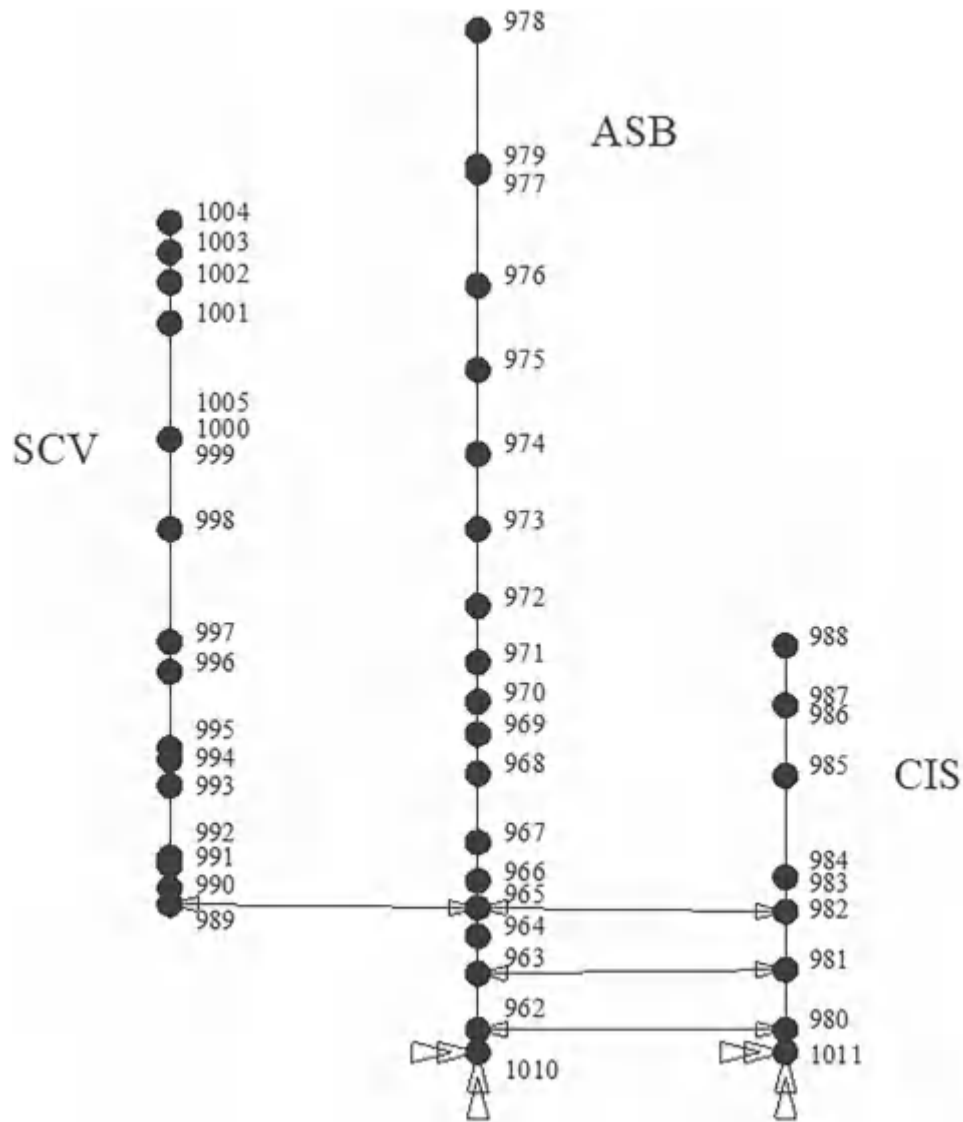
FIGURE 1 AP1000 finite element mass stick model. ASB, auxiliary and shield building; CIS, containment internal structures; SCV, steel containment vessel
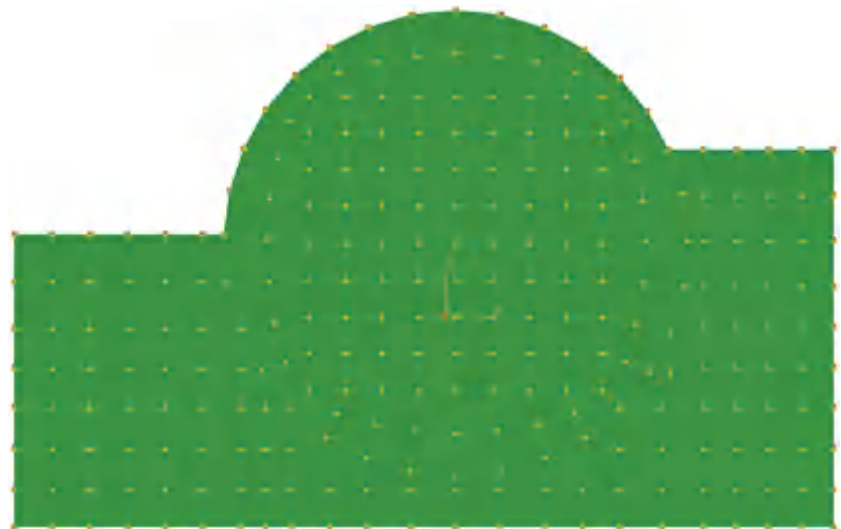

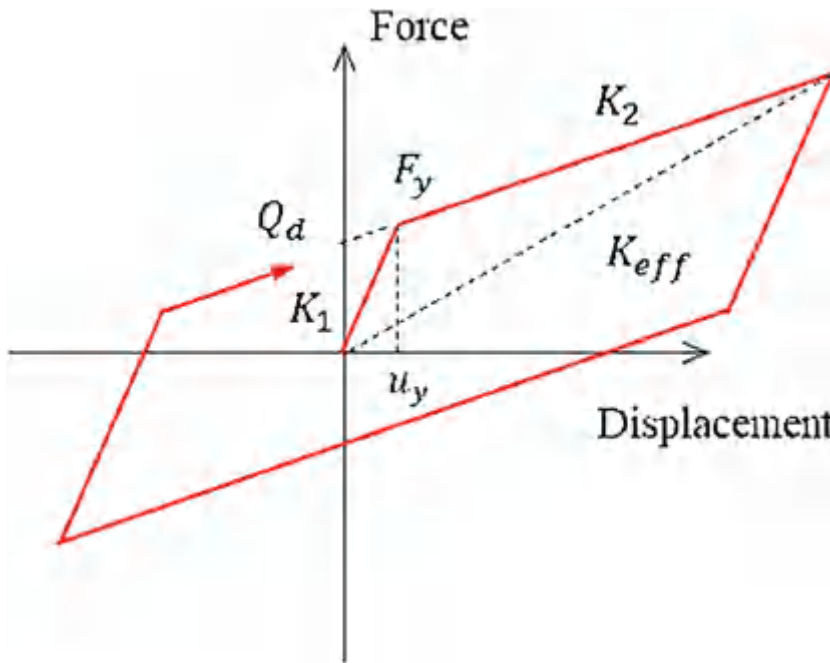**FIGURE 2** Layout of lead-rubber bearing in AP1000

FIGURE 3 Bilinear model of lead-rubber bearing

TABLE 1 Frequency comparison of non-isolated and isolated AP1000 model

Non-isolated model			Isolated model		
Remarks	Mode No.	Frequency (Hz)	Remarks	Mode No.	Frequency (Hz)
ASB 1st Translation in the X Direction	1	3.29	Isolation 1st Translation in the X Direction	1	0.49
ASB 1st Translation in the Y Direction	2	3.60	Isolation 1st Translation in the Y Direction	2	0.49
SCV 1st Translation in the X Direction	5	5.92	Isolation 1st Torsion in the X Direction	3	0.57
SCV 1st Translation in the Y Direction	7	6.64	ASB 1st Translation in the X Direction	4	3.53
CIS 1st Translation in the X Direction	13	11.62	ASB 1st Translation in the Y Direction	6	3.85
CIS 1st Translation in the Y Direction	14	12.00	SCV 1st Translation in the X Direction	8	5.98
-	-	-	SCV 1st Translation in the Y Direction	10	6.74
-	-	-	CIS 1st Translation in the X Direction	16	11.91
-	-	-	CIS 1st Translation in the Y Direction	18	13.56

Abbreviations: ASB, auxiliary and shield building; CIS, containment internal structures; SCV, steel containment vessel.

isolation bearings when changing each parameter, solely presenting the first quadrant. Herein, K_2 correlates to property of rubber, the effective diameter of rubber bearing, and the total thickness of rubber layers at a given specified height of the bearing. Q_d is influenced by the properties and diameter of the lead plug. K_1 is more associated with the diameter of the lead plug.

2.3 | Ground motion selection and adjustment

Different kinds of inputted ground motion result in varying seismic response of NPPs. The US Nuclear Regulatory Commission requires seismic design of NPPs satisfy seismic response spectrum in Regulatory Guide 1.60[25]. It is also noted that ground motions can be selected corresponding to ATC-58 in US specification [26] and research results of Huang[27] for sake of safety. As shown in Figure 5, "geometric-mean scaling method" was used to scale the selected 20 motions, taking several structural frequencies into consideration, rather than the basic frequency. Figure 6 illustrates the 5% damped response spectra associated with Regulatory Guide 1.60 (including high frequency enrichment) corresponding to PGA being 0.5 g. The information of the selected motions is illustrated in Table 2.

Isolation frequency, ASB fundamental frequency, SCV fundamental frequency, and CIS fundamental frequency are taken as key frequencies for considering the influence of isolation mode and structure mode. The designed isolation frequency is 0.49 Hz, while the fundamental frequencies of ASB, SCV, and CIS are 3.53, 5.98, and 11.91 Hz, respectively. In addition, to jugde the discreteness of ground motions, it is assumed that the ground motion amplitudes are lognormally distributed. Herein, 16th, 84th, 5th, and 95th percentile spectral ordinates are marked as y_{16th}, y_{84th}
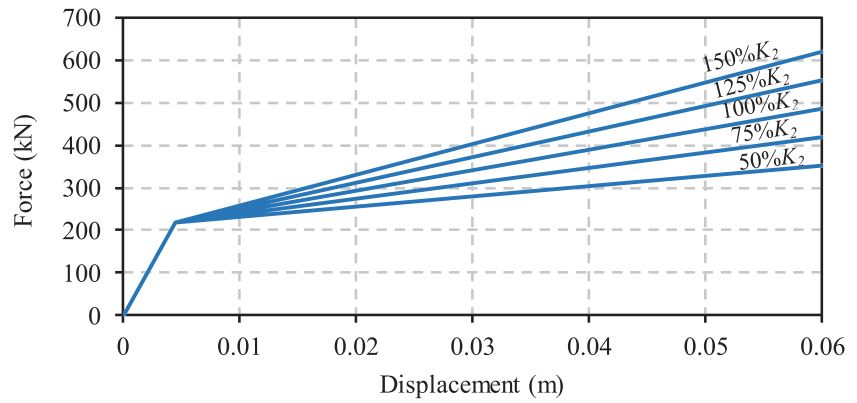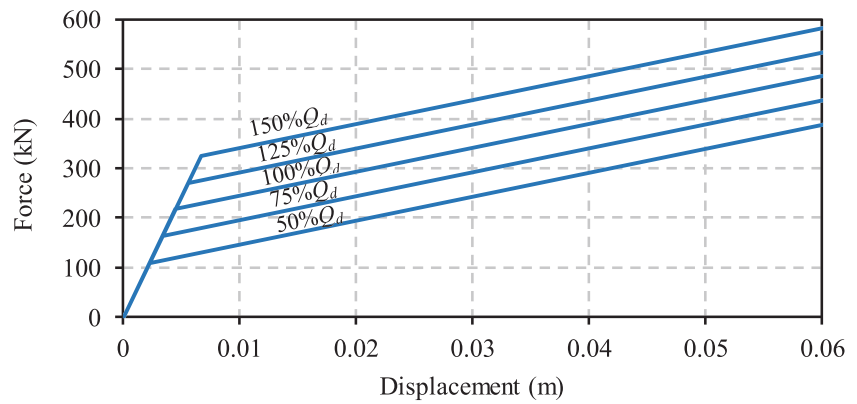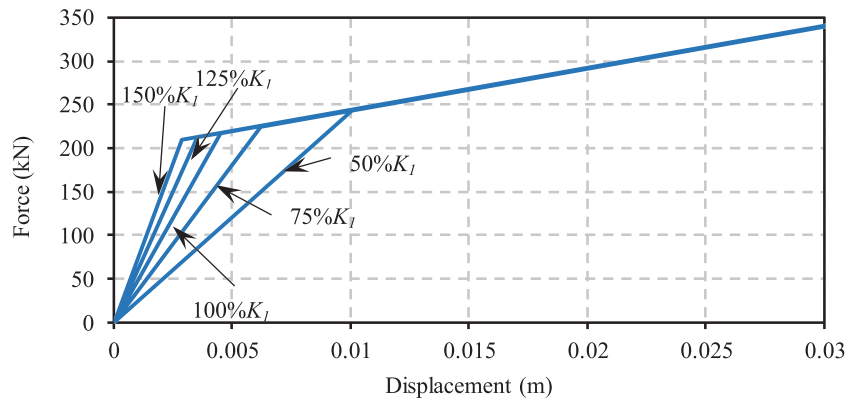
(a) Force-displacement curve under varying K_2

(b) Force-displacement curve under varying Q_d

FIGURE 4 Force-displacement curve of isolation bearings varying K_2 (a), Q_d (b), and K_1 (c)

(c) Force-displacement curve under varying K_1

y_{5th}, and y_{95th}, respectively [23]. The related calculation methods are listed in Equations 1 to 6. Where n is the number of selected ground motions, which is 20 in this case. θ and β are the mean value and the standard deviation of the amplitudes of the selected motions. y_i is the value of spectral acceleration of the ith ground motion at a given period. The 84th percentile spectral ordinate corresponds to the value shifting one standard deviation from the mean value. The 95th percentile spectral ordinate satisfies both Chinese and American standards, ensuring engineering application meaningfully. In this study, the selected 20 tri-axial motions were applied to AP1000 model so as to study the comprehensive influence of key parameters on seismic response of the nuclear structures.

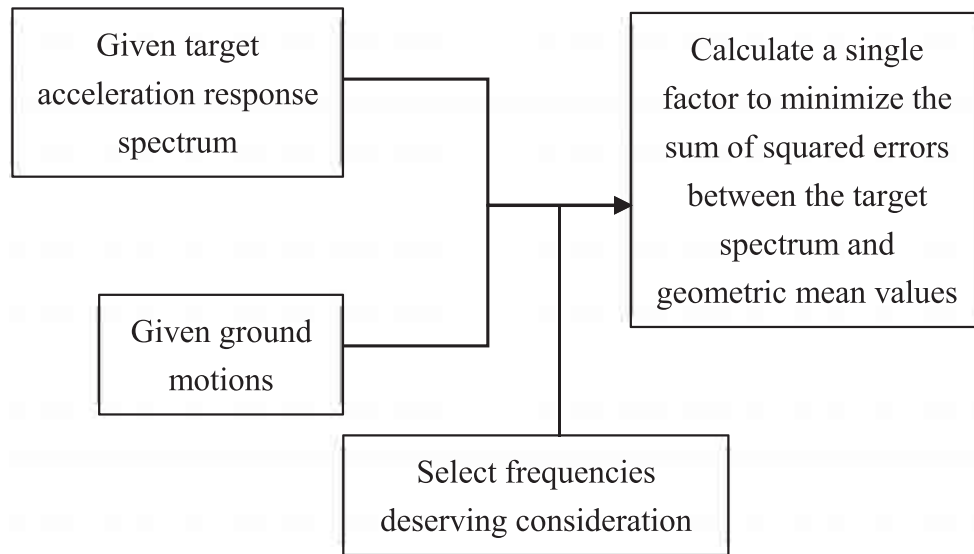$$\theta = \exp\left(\frac{1}{n}\sum_{i=1}^{n}\ln(y_i)\right) \tag{1}$$
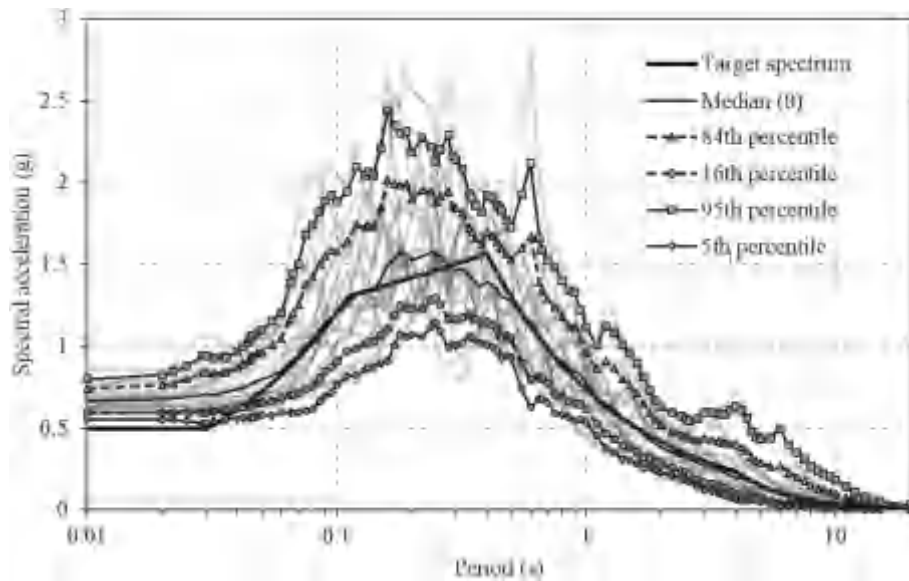
FIGURE 5 Geometric-mean scaling method

FIGURE 6 Spectral acceleration of selected motions

$$\beta = \sqrt{\frac{1}{n}\sum_{i=1}^{n}(\ln(y_i)-\ln(\theta))^2} \tag{2}$$

$$y_{16th} = \theta e^{-\beta} \tag{3}$$

$$y_{84th} = \theta e^{\beta} \tag{4}$$

$$y_{5th} = \theta e^{-1.645\beta} \tag{5}$$

$$y_{95th} = \theta e^{1.645\beta} \tag{6}$$

TABLE 2   Information of selected motions

Record No.	NGA No. & Earthquake	Station	Magnitude	Epicentral distance (km)	Scaling factor
1	68 San Fernando	LA-Hollywood Stor FF	6.6	22.8	3.45
2	93 San Fernando	Whittier Narrows Dam 6.6	6.6	39.5	7.47
3	186 Imperial Valler-06	Niland Fire Station	6.5	36.9	7.64
4	285 Irpinia,Italy-01	Bagnoli Irpinio	6.9	8.2	3.78
5	718 Superstition Hills-01	Wildlife Liquef. Array	6.2	17.6	4.77
6	730 Spitak, Armenia	Gukasian	6.8	36.2	3.74
7	748 Loma Prieta	Belmont-Envirotech	6.9	44.1	6.27
8	855 Landers	Fort Irwin	7.3	63.0	6.08
9	862 Landers	Indio-Coachella Canal	7.3	54.3	5.84
10	882 Landers	North Palm Springs	7.3	26.8	4.36
11	1165 Kocaeli, Turkey	Izmit	7.5	7.2	3.05
12	1487 Chi-Chi, Taiwan	TCU047	7.6	35.0	1.94
13	1491 Chi-Chi, Taiwan	TCU051	7.6	7.7	3.05
14	1602 Duzce, Turkey	Bolu	7.1	12.0	1.09
15	1605 Duzce, Turkey	Duzce	7.1	6.6	1.43
16	1611 Duzce, Turkey	Lamont 1058	7.1	0.2	8.14
17	1762 Hector Mine	Amboy	7.1	43.1	3.32
18	2113 Denali, Alaska	TAPS Pump Station #09	7.9	54.8	10.67
19	2744 Chi-Chi, Taiwan-04	CHY088	6.2	48.4	7.92
20	3264 Chi-Chi, Taiwan-06	CHY024	6.3	31.1	4.51

3 | NUMERICAL ANALYSIS OF SEISMIC RESPONSE

3.1 | Seismic response of AP1000 model

3.1.1 | Acceleration response

The top nodes of three sticks are at different elevations, and the acceleration response there is representative. Figure 7 presents the spectral acceleration at the top nodes of three sticks when changing K_2, Q_d, and K_1. Herein, spectral acceleration represents mean response under 20 ground motions, reflecting seismic response at an average level.

The black line named "fixed" represents the acceleration response under non-isolation. It is noticeable that isolation system decreases the acceleration response by a large margin at fundamental frequency of sticks while amplifies the acceleration response slightly at isolation frequency. After isolation, acceleration response spectra at top nodes have two remarkable extremums at isolation frequency and fundamental frequency of sticks. Nevertheless, it can be concluded that the application of isolation bearings successfully achieves remarkable isolation effects.

The impact degree of three key parameters on spectral acceleration is analyzed. K_1 has little effect on the AP1000 acceleration response spectrum. In the case that K_1 increased from 50 to 150%, spectrum values at isolation frequency decreased by 4.7%, and spectrum values at sticks fundamental frequency increased by 17.3% (ASB), 45.6% (SCV), and 17.0% (CIS).

The gradual increase of K_2 results in increase of isolation frequency, as well as the increase of corresponding peak acceleration response. Quantitatively, isolation frequency increased a half approximately, and the spectrum value at isolation frequency increased about 150%. This is because equivalent stiffness of isolation bearings amplifies with the gradual increase of K_2. Secondary, within the scope of K_2 increment, the occurrence of the peak spectral acceleration always occurs at fundamental frequency in ASB and SCV, while the position of peak spectral acceleration witnesses a change in CIS. It shows peak spectral acceleration response occurs at fundamental frequency when K_2 is smaller than 4,828.43 kN/m in CIS while occurs at isolation frequency otherwise.

Spectral accelerations at isolation frequency and sticks fundamental frequency show different tendency with different Q_d. Spectral accelerations at isolation frequency decrease, and spectral accelerations at sticks fundamental frequency increase when raising Q_d. The position of peak spectral acceleration exists a change in SCV and CIS when changing Q_d, while the occurrence holds at fundamental frequency in ASB. With the increase of Q_d, spectral acceleration at fundamental frequency of sticks ASB and SCV rises while declines about 12–13% at isolation frequency, as equivalent stiffness improves slightly under this condition.
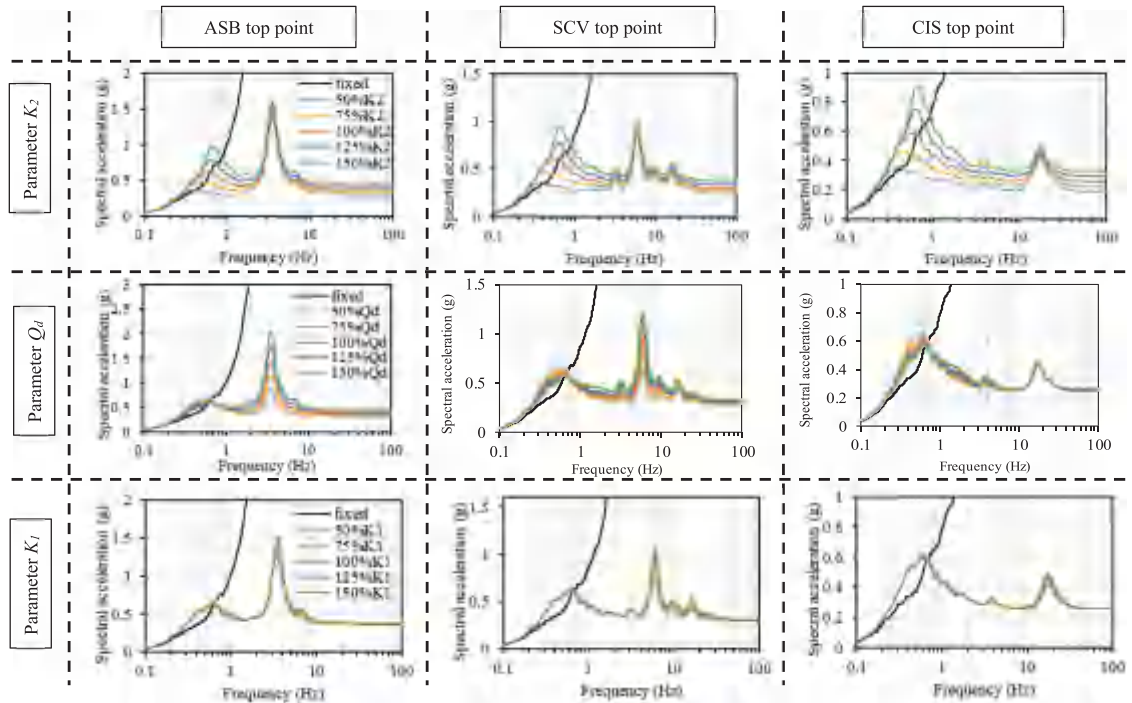
FIGURE 7 Impact of different parameters on spectral acceleration at top points of three sticks. ASB, auxiliary and shield building; CIS, containment internal structures; SCV, steel containment vessel

In comparison of three key parameters, K_2 has a most remarkable impact on spectral acceleration on the isolation frequency, and Q_d has a most remarkable impact on spectral acceleration on the fundamental frequency of sticks ASB and SCV.

3.1.2 | Seismic mitigation efficiency

In order to research on the seismic mitigation efficiency of isolation system quantitatively, two indexes are defined: the ratio of top maximum acceleration between isolated and non-isolated models (ζ_1) and the ratio of maximum deformation between isolated and non-isolated models (ζ_2). The maximum deformation is defined by the maximum difference of displacement between top point and bottom point of the three sticks. The detailed information of seismic mitigation efficiency when changing key parameters is listed in Table 3. Table 4 presents maximum top acceleration and deformation of ASB, CSV, and CIS of non-isolated model. Similarly, all values involved here are mean values under 20 seismic waves.

In non-isolated model, SCV has the highest peak acceleration (5.15 g), and ASB has the biggest deformation (0.083 m). After the application of isolation bearings, both the peak acceleration and stick deformation achieve significant decline. As a result, SCV achieves the most seismic mitigation efficiency in term of peak acceleration and deformation of ASB achieves the same in terms of deformation. As a relatively rigid structure, both the peak acceleration and deformation of CIS are smaller, which in turn causes lower seismic mitigation efficiency of CIS.

The impact of each parameter on seismic mitigation efficiency is concerned. The increase of K_2 reduces the seismic mitigation efficiency, and CIS is most sensitive to the increase of K_2, with nearly 50% decrease of seismic mitigation efficiency. The results show that the increase of Q_d reduces seismic mitigation efficiency in ASB and SCV, which shows inversely in CIS. The influence of K_1 is quite slight, with the seismic mitigation efficiency almost invariant.

3.1.3 | Discreteness of seismic response

Figures 8 and 9 describe the discreteness of top point acceleration and deformation of three sticks. The statistical analysis of acceleration and deformation utilizes peak values during time history. Median, 95th, 84th, 16th, and 5th percentile values are presented assuming that maximum values obtained from the response history analysis are lognormally distributed. In each subgraph, the short horizontal lines are sorted in descending percentile value order and the intervals between them visualize discreteness.

Comparing the line named "fixed" with others, it is noticeable that the use of isolation system leads to very significant reductions in the average and discreteness of maximum acceleration and deformation. The impact extent of the key parameters on discreteness has been studied. When changing K_2 from 50 to 150%, mean accelerations of three top nodes all tend to increase, accompanying larger discreteness. When changing

TABLE 3 Impact of different parameters on seismic mitigation efficiency

Isolator parameters	Ratio of maximum acceleration between isolated and non-isolated models on the top points (ζ_1)			Ratio of maximum deformation between isolated and non-isolated models (ζ_2)		
	ASB top	CIS top	SCV top	ASB	CIS	SCV
50%K_2	9.07%	11.80%	6.59%	13.06%	23.16%	13.72%
75%K_2	10.14%	14.60%	7.38%	15.60%	29.04%	16.90%
100%K_2	11.42%	16.97%	8.28%	18.18%	33.79%	19.48%
125%K_2	12.70%	19.49%	9.26%	20.76%	38.47%	22.34%
150%K_2	14.69%	22.11%	10.62%	23.53%	43.35%	25.33%
50%Q_d	10.22%	17.75%	8.16%	17.89%	35.02%	19.86%
75%Q_d	10.73%	17.30%	8.22%	17.90%	34.33%	19.62%
100%Q_d	11.42%	16.97%	8.28%	18.18%	33.79%	19.48%
125%Q_d	12.17%	16.68%	8.41%	18.60%	33.47%	19.48%
150%Q_d	13.08%	16.44%	8.60%	19.14%	33.21%	19.58%
50%K_1	11.15%	17.07%	7.98%	18.17%	33.97%	19.51%
75%K_1	11.33%	17.01%	8.14%	18.15%	33.84%	19.48%
100%K_1	11.42%	16.97%	8.28%	18.18%	33.79%	19.48%
125%K_1	11.51%	16.96%	8.44%	18.18%	33.76%	19.50%
150%K_1	11.56%	16.97%	8.61%	18.19%	33.75%	19.54%

Abbreviations: ASB, auxiliary and shield building; CIS, containment internal structures; SCV, steel containment vessel.

TABLE 4 Maximum peak acceleration and deformation of non-isolated model (0.5g)

Remarks	Maximum acceleration (g)			Maximum displacement (m)		
	ASB top	CIS top	SCV top	ASB top	CIS top	SCV top
Response	4.09	2.30	5.15	0.083	0.0041	0.032

Abbreviations: ASB, auxiliary and shield building; CIS, containment internal structures; SCV, steel containment vessel.

Q_d, mean accelerations tend to increase, and the discreteness increases in ASB while decreases in CIS. When it comes to the deformation, it shows that only K_2 gives rise to striking changes, whose changing tendency features similar to those of acceleration. By contrast, the influence of K_1 on both acceleration and deformation is less significant.

After isolation, the top node of ASB bears the fastest acceleration (0.420 g), while its discreteness is the smallest, and that of CIS has the slowest acceleration (0.304 g), while the discreteness is the largest. This can be explained in Figure 10, combining the acceleration response inputted into the top of isolation bearings. The difference of acceleration response values between 95 and 5% spectral ordinates are 0.296 g (ASB), 0.323 g (SCV), and 0.346 g (CIS), that is, the biggest input acceleration response discreteness leads to the biggest output discreteness.

3.2 | Seismic response of isolation bearings

In this section, the impact on isolation bearings under different key parameters are focused. Mean values of indexes including average of peak deformation, maximum deformation, average equivalent stiffness, and average natural period of isolators with parameters changing are shown in Table 5. Herein, the equivalent stiffness and natural period are calculated by maximum deformation of isolation bearings. It is noticeable that K_2 accounts for the most significant influence, then Q_d and K_1 in turn. When increasing K_2 ranging from 50 to 150%, both the average and maximum deformation of isolation bearings decrease, especially the maximum deformation. Simultaneously, the value of mean equivalent stiffness reaches more than double, and value of mean equivalent period changes from 2.68 to 1.66 s. When it comes to integral influential effect of key parameters, K_2 has the most significant influence on both superstructure and isolation bearings, that is, more attention ought to be paid on K_2 when considering peak isolator deformation.
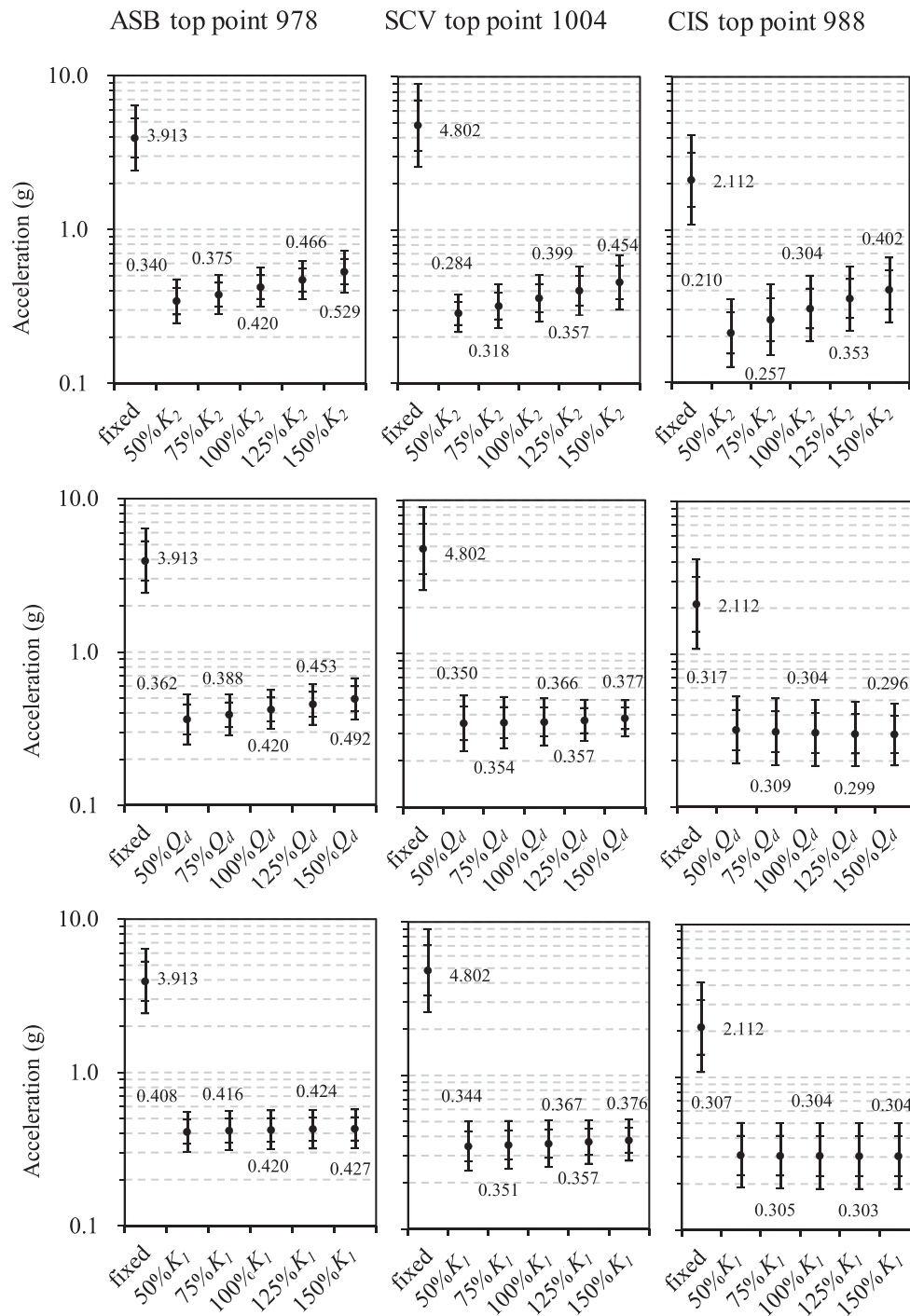
FIGURE 8 Impact of different parameters on discreteness of peak acceleration at top points of three sticks. ASB, auxiliary and shield building; CIS, containment internal structures; SCV, steel containment vessel

3.3 | Performance space

In design of structure isolation system, it is ideal to low down the acceleration of sticks and control the relative deformation of isolation bearings within a reasonable range simultaneously. But under real earthquake exaction, the two parameters may not achieve optimal state simultaneously. The performance space is an effective method to investigate the relative relationship of the two chosen indices of interest, illustrated in Huang [18]. Herein, the joint probability density function (JPDF) of the two parameters is assumed to be jointly lognormal. The peak acceleration of sticks and the deformation of LRB are denoted as two random variables, X and Y, respectively. The JPDF of X and Y is calculated by Equation 7.
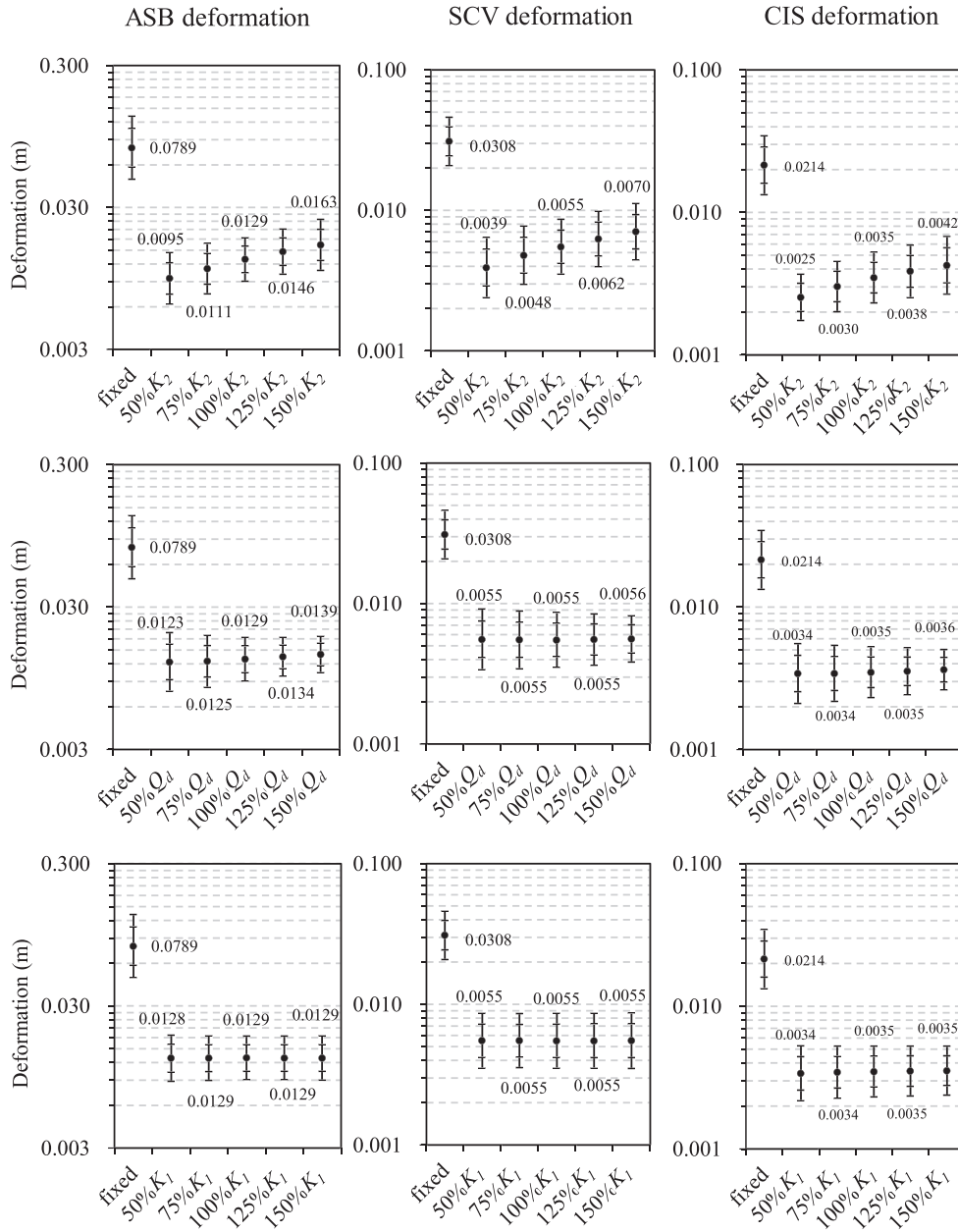
FIGURE 9   Impact of different parameters on discreteness of deformation of three sticks. ASB, auxiliary and shield building; CIS, containment internal structures; SCV, steel containment vessel

$$f_{XY} = \frac{1}{2\pi \cdot xy \cdot |\Lambda|^{0.5}} \exp\left[-0.5 \cdot (\tilde{z} - \tilde{m})^T \Lambda^{-1} (\tilde{z} - \tilde{m})\right] \qquad (7)$$

where $\tilde{z} = [\ln(x); \ln(y)]^T$. The factors $\tilde{m}$ and Λ are the mean vector and covariance matrix of random variables $\ln(x)$ and $\ln(y)$ and can be calculated by the sample points which are seismic response under the 20 ground motions. Herein, two kinds of JPDFs are applied for different purposes. In Case 1, the maximum acceleration of stick top and deformation of LRB are set as the two parameters, pursuing for lower peak acceleration within the limited range of isolator deformation. In Case 2, the maximum acceleration of stick top and the deformation of ASB are set as the two parameters to control the seismic response from a comprehensive perspective. Figures 11 and 12 illustrate the calculation procedure. Figures 11a and 12a show the JPDF in Cases 1 and 2. The total volume under the surface of the JPDF function is 1; the area in the XY plane corresponding to 84% of the total volume is the performance space of Figures 11b and 12b, which also show all the 20 response result points from response history analysis.
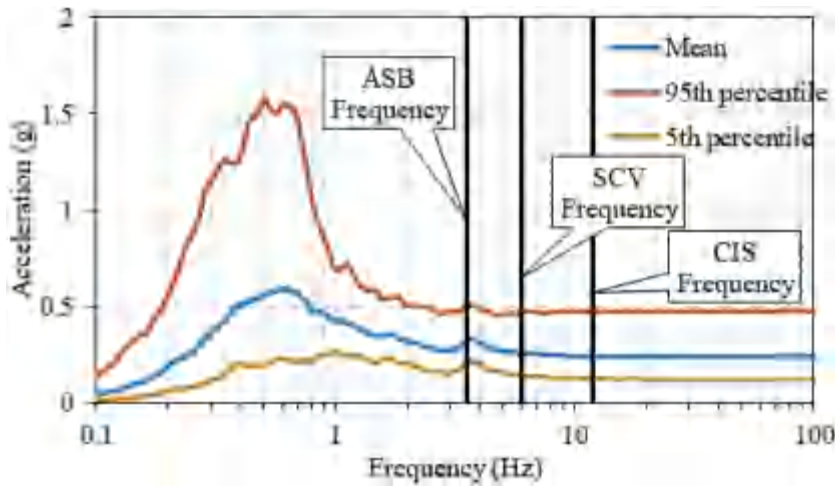
FIGURE 10   Spectral acceleration in X direction at the top of isolation plane. ASB, auxiliary and shield building; CIS, containment internal structures; SCV, steel containment vessel

TABLE 5   Impact of different parameters on isolators performance

Isolation parameters	Average of peak isolator deformation (m)	Maximum deformation of isolator (m)	Average effective stiffness of isolator (kN/m)	Average natural periods of isolator (s)
50%K_2	0.378	0.896	3060.2	2.68
75%K_2	0.340	0.668	4298.8	2.26
100%K_2	0.314	0.513	5527.4	1.99
125%K_2	0.297	0.488	6744.9	1.80
150%K_2	0.284	0.458	7961.7	1.66
50%Q_d	0.330	0.550	5161.3	2.06
75%Q_d	0.321	0.532	5342.5	2.02
100%Q_d	0.314	0.513	5527.4	1.99
125%Q_d	0.307	0.499	5718.7	1.96
150%Q_d	0.301	0.482	5914.5	1.93
50%K_1	0.315	0.517	5526.3	1.99
75%K_1	0.314	0.515	5527.3	1.99
100%K_1	0.314	0.513	5527.4	1.99
125%K_1	0.314	0.515	5528.3	1.99
150%K_1	0.313	0.514	5528.2	1.99
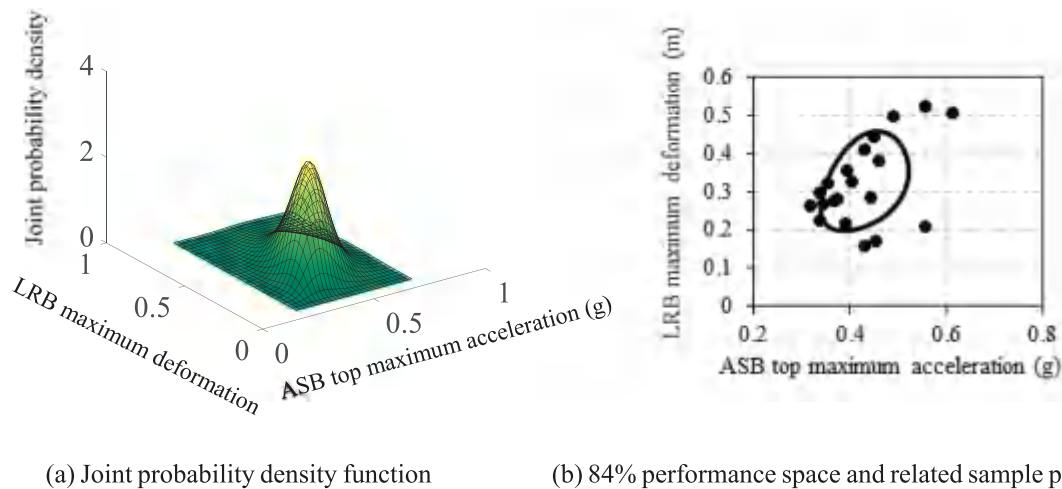
(a) Joint probability density function   (b) 84% performance space and related sample points

FIGURE 11   Joint probability density function (a) and 84% performance space and related sample points (b) of Case 1. ASB, auxiliary and shield building; LRB, lead-rubber bearing
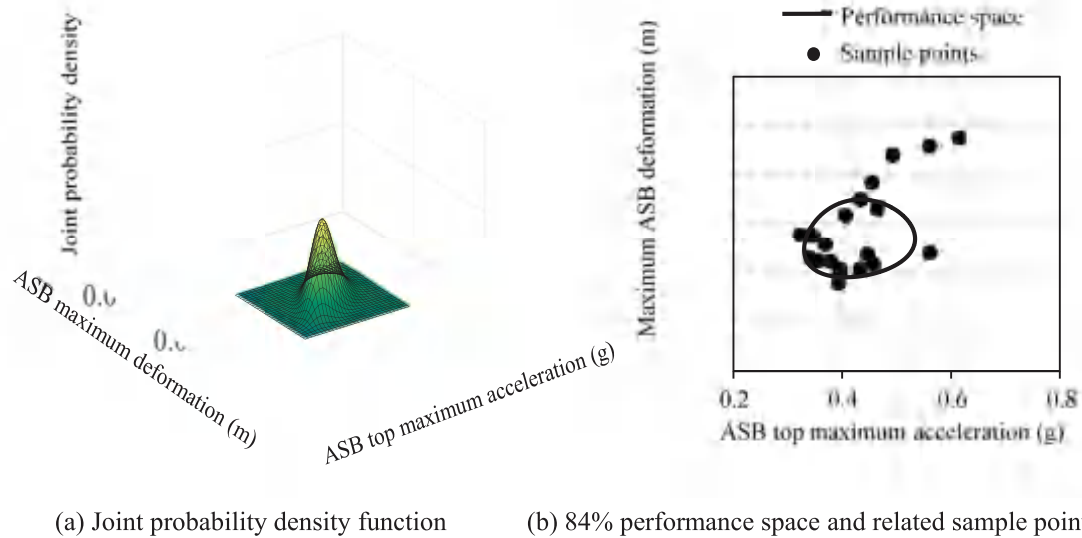
(a) Joint probability density function   (b) 84% performance space and related sample points

FIGURE 12 Joint probability density function (a) and 84% performance space and related sample points (b) of Case 2. ASB, auxiliary and shield building

Figures 13 and 14 present performance space of average response of three sticks with 5% damping ratio. The central asterisk point represents the top point of the JPDF projected to the horizontal plane. The results have been summarized as followed:

1. The above figures show that K_2 has the most significant impact on performance space. It is clear that the maximum acceleration and deformation of sticks increase, and the deformation of isolation bearings decreases, when increasing K_2. In Case 1, with the increase of K_2, the range of LRB deformation reduced while that of top peak acceleration increased. In Case 2, both the ranges of acceleration and deformation increase. It is noted that the change in range of top peak acceleration and deformation correctly corresponds to the above analysis of discreteness in Section 3.1.3.
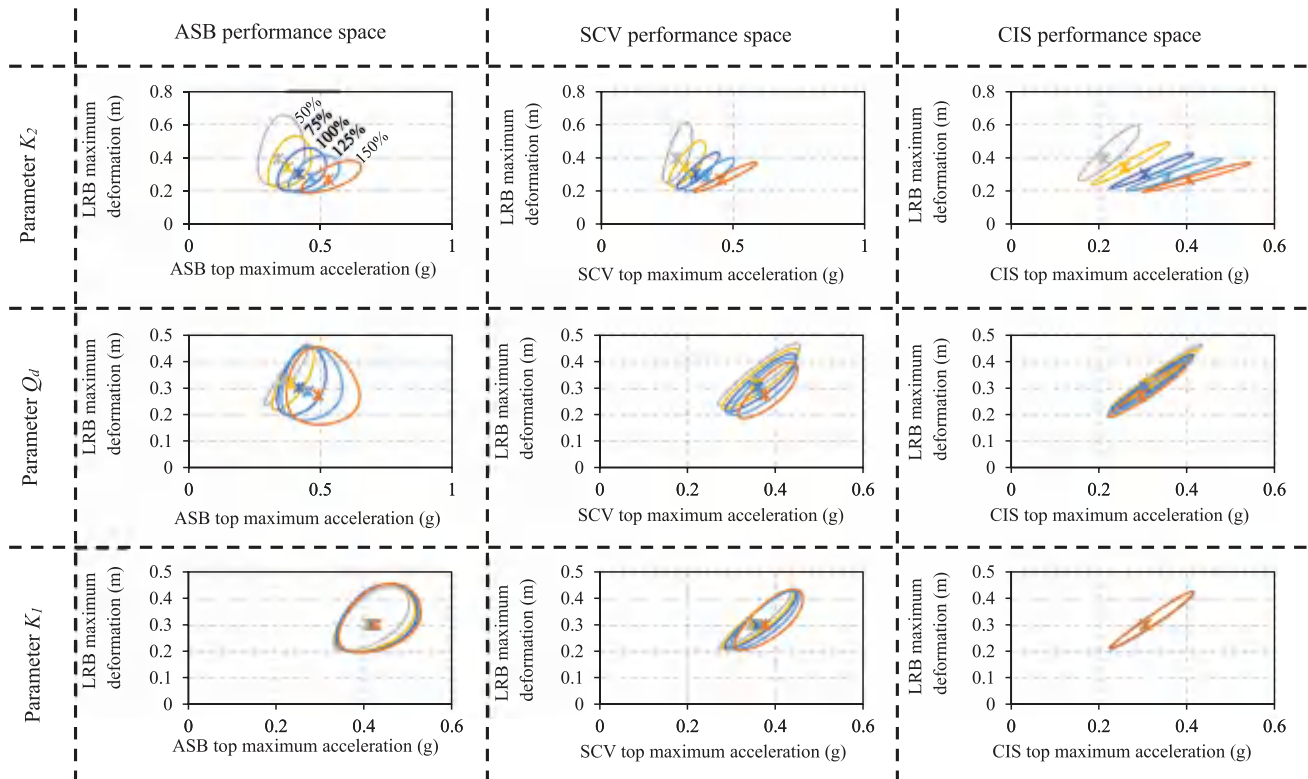

FIGURE 13 Impact of different parameters on performance space for Case1. ASB, auxiliary and shield building; CIS, containment internal structures; LRB, lead-rubber bearing; SCV, steel containment vessel
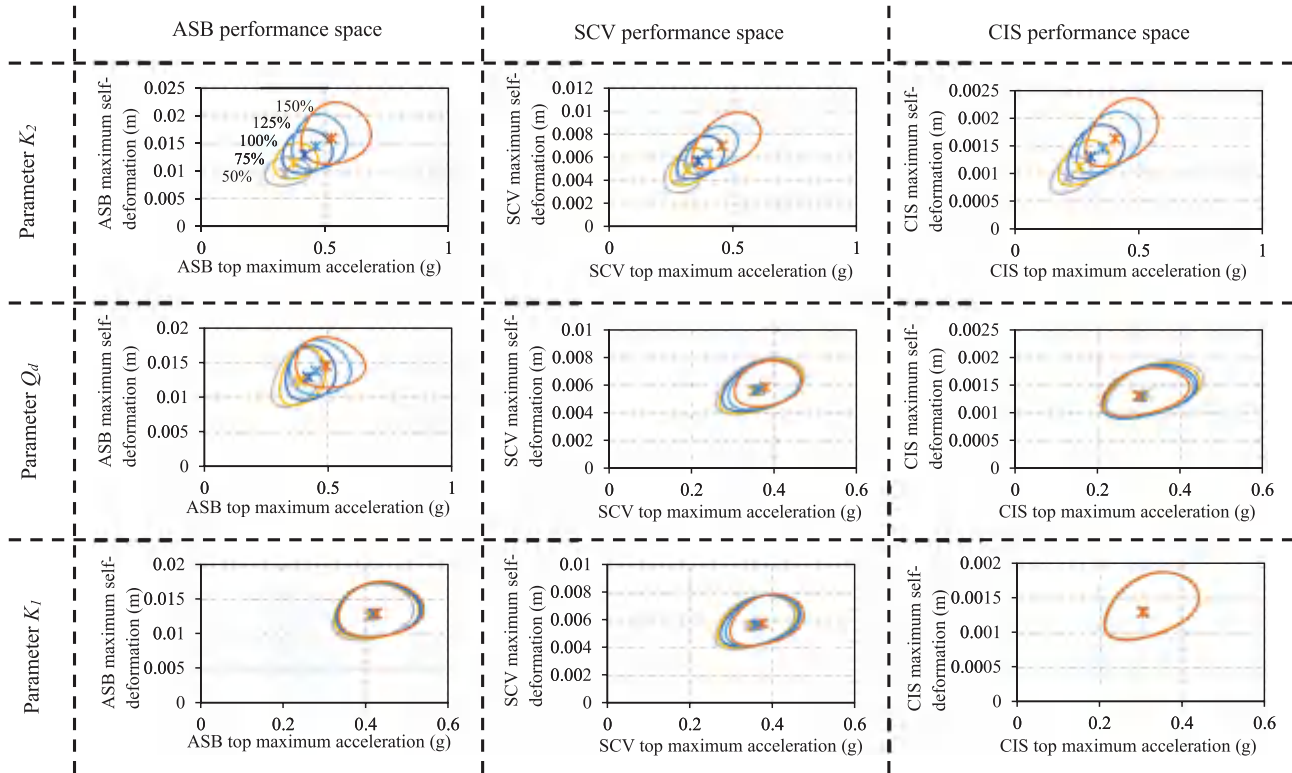
FIGURE 14 Impact of different parameters on performance space for Case2. ASB, auxiliary and shield building; CIS, containment internal structures; SCV, steel containment vessel
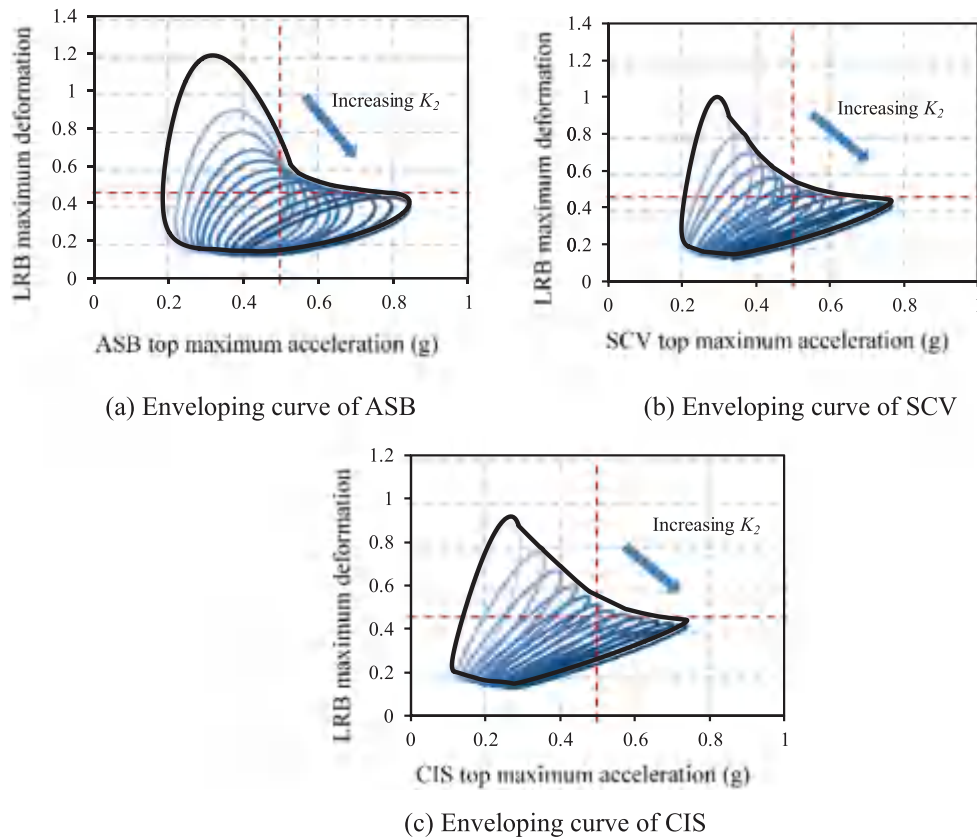

(a) Enveloping curve of ASB

(b) Enveloping curve of SCV

(c) Enveloping curve of CIS

FIGURE 15 Enveloping curve of ASB (a), SCV (b), CIS (c) when changing K_2. ASB, auxiliary and shield building; CIS, containment internal structures; LRB, lead-rubber bearing; SCV, steel containment vessel

2. Q_d has a more obvious impact on ASB, where peak acceleration and deformation increase, while deformation of LRB declines. The changing tendency of SCV is similar to that of ASB, though much slighter. Conversely, the increase of Q_d brings top peak acceleration and deformation of CIS down slightly. When it comes to the range of seismic response, the influence of Q_d varies under different conditions. In Case 1, with the increase of Q_d, ranges of acceleration and deformation of LRB increase in ASB, while those in SCV decrease. The range of deformation decreases and that of acceleration has no obvious change in CIS. In Case 2, the increase of Q_d lows down the range of deformation slightly both in ASB and SCV and almost has no impact on CIS.

3. When changing K_1 ranging from 50 to 150% of the initial value, there is nearly no remarkable change in the range of LRB maximum deformation. A slight increase occurred on peak acceleration and deformation of ASB and SCV. All indicators of CIS are very insensitive to K_1.

4. Viewed from a general perspective, given a specified deformation of LRB, ASB shows a wider acceleration range than SCV and CIS. This means there is a higher possibility for designers to estimate acceleration range of SCV and CIS accurately within a certain LRB deformation restrict.

3.4 | Performance curve boundary

In actual engineering design, it is of great importance to make sure to what extent could the acceleration reduces when satisfying the requirement of isolator deformation. Besides, in complex cases like the AP1000 model, there is a need for designers to gain a general idea of the range of peak acceleration response under a given deformation, even during the early period of isolation design. In order to obtain the envelope diagram of performance curves, in this section, additional numerical analysis of changing K_2 and Q_d was performed. To be more specific, K_2 is changed ranging from 37.5 to 175% of its initial value, with a step of 25%. When it comes to Q_d, it is necessary to control yield-to-weight ratio (the ratio of total yield force of all isolation bearings and the weight of superstructure in AP1000) within the range of 0.01 to 0.1. Thus, 22.5, 56.4, 73.3, 90.2, 107.1, 124.0, 140.9, 157.8, 174.8, 191.7, 208.6, and 225.5% of Q_d were added.
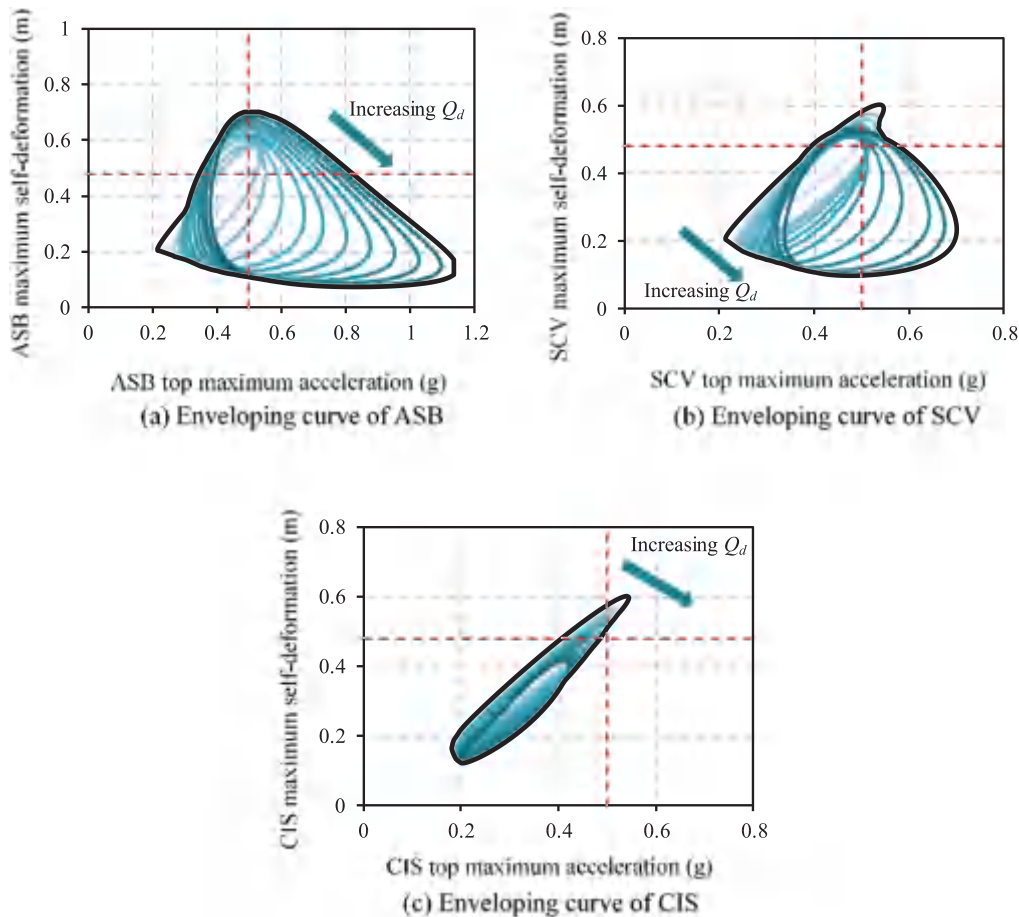

FIGURE 16   Enveloping curve of ASB (a), SCV (b), CIS (c) when changing Q_d. ASB, auxiliary and shield building; CIS, containment internal structures; SCV, steel containment vessel

Figures 15 and 16 present the envelope curves of performance space with varying parameters, and the black line represents envelops. Herein, the performance space is under 95% confidence interval, guaranteeing relatively high safety in practical engineering design. The rubber layer thickness t_r and diameter d of LRB are set as 16 cm and 1.4 m for the initial isolation parameters. According to Equation 8, the maximum deformation of LRB, u_{max}, equals 0.48 m, marked in red horizontal dashed line in Figures 15 and 16. The red vertical dashed line represents the supposed limit of peak acceleration response (0.5 g).

$$u_{max} \leq \min\{0.55d; 3t_r\} \tag{8}$$

With K_2 changed in Figure 15, the minimum accelerations in ASB, SCV, and CIS can reduce to 0.18, 0.20, and 0.11 g, respectively. Additionally, the minimum deformation of LRB can reach 0.14 m. By analysis, it shows the deformation of LRB can be controlled under 0.48 m, and the maximum peak acceleration can be controlled under 0.5 g in SCV and CIS, with 95% probability. With Q_d changing in Figure 16, the minimum accelerations in ASB, SCV, and CIS reduce to 0.22, 0.21, and 0.18 g, respectively.

4 | CONCLUSIONS

With the increasingly utilization of nuclear power, the public tends to pay more attention to the safety of NPPs, whose potential threats are no doubt catastrophic. Effective isolation measures manage to alleviate damages caused by earthquakes, but there are still lack of enough research on quantitative analysis of characteristic parameters in the field of isolation design. In this paper, a three-stick model of AP1000 in ABAQUS was built, and a series of numerical analysis under 20 selected strong ground motions were carried out. Peak acceleration response of top points, deformation of each stick and deformation of LRB are taken into consideration. Furthermore, the conception of performance space on the basis of JPDF was utilized, to control two related seismic response within an acceptable range, Conclusions are drawn below:

1. The seismic response is more sensitive to K_2 and Q_d. When changing K_2 from 50% to 150% of its initial value, isolation frequency increases, and the corresponding acceleration response can reach up to nearly 2.5 times in all sticks. The increase of Q_d in the same magnitude increases the spectral acceleration response at stick fundamental frequency and reduces it at the isolation frequency.

2. The optimal seismic mitigation efficiency of isolation occurs in the sticks with corresponding maximum acceleration and deformation under non-isolated condition, that is, SCV achieves the optimal acceleration mitigation efficiency, and ASB achieves the optimal deformation mitigation efficiency.

3. Isolation succeeds in reducing the discreteness of seismic response largely, and the influence degree varies based on characteristics of sticks and parameters of isolators.

4. The performance space method is introduced as one means of achieving an optimal situation, when both the two related variables meet regulatory requirements. The advantage of performance space method is that it can present the changing range and tendency of two related variables simultaneously. Envelope diagram of performance curves can be applied to estimate the possible range of isolator parameters when satisfying the requirements.

5. It is clear that isolation significantly reduces both the mean value and discreteness of seismic response. In isolation design of AP1000, it is imperative to understand the impact of different parameters giving rise to and pay attention to the inputted response spectra.

ORCID

Zhiguang Zhou https://orcid.org/0000-0002-2799-0724

REFERENCES

[1] R. L. Mayes, M. R. Button, D. M. Jones, Proceedings of Structural Engineering World Congress, CA, San Francisco 1998.

[2] M. Forni, A. Poggianti, A. Dusi. Proceedings of 15th World Conference on Earthquake Engineering, Lisbon (Portugal), 2012.

[3] A. S. Whittaker, M. Kumar, M. Kumar, Nucl. Eng. Technol. 2014, 46(5), 569.

[4] F. G. Fan, G. Ahmadi, Eng. Struct. 1992, 14(1), 35.

[5] H. Khechfe, M. Noori, Z. Hou, J. M. Kelly, G. Ahmadi, J. Pressure Vessel Technol (ASME) 2002, 124(1), 81.

[6] J. Zhang, Y. L. Huo, Eng. Struct. 2009, 31, 1648.

[7] J. Wong, A. Schellenberg, S. Mahin. 13th World Conference on seismic isolation, energy dissipation and active vibration control of structures, Sendai Japan, 2013.

[8] N. M. Amin, N. Ayub, A. Alisibramulisi, International Journal of GEOMATE 2019, 63(17), 23.

[9] D. C. Charmpis, P. Komodromos, M. C. Phocas, Earth. Eng. Struct. D. 2012, 41(15), 2289.

[10] D. C. Charmpis, M. C. Phocas, P. Komodromos, B. Earthq. Eng. 2015, 13(9), 2745.

[11] A. Ali, N. A. Hayah, D. Kim, et al., Nucl. Eng. Technol. 2014, 46(5), 699.

[12] J. M. Kelly, Report No.UCB/EERC-81/17, Earthquake Engineering Research Center, College of Engineering, University of California, Berkeley, CA 1982.

[13] J. M. Kelly, H. C. Tsai, Report No.UCB/SESM-84/17, Division of Structural Engineering and Structural Mechanics, Department of Civil Engineering, College of Engineering, University of California, Berkeley, CA 1984.

[14] B. K. Roy, S. Chakraborty, S. K. Mihsra, J. Vib. Contorl. 2014, 20(5), 786.

[15] R. S. Jangid, Eng. Struct. 2005, 27(3), 349.

[16] C. P. Providakis, Eng. Struct. 2008, 30(5), 1187.

[17] G. S. Sun, A. Q. Li, J. Southeast University. 2009, 39(2), 320.

[18] M. Kumar, A. Whittaker, M. Constantinou, Seismic isolation of nuclear power plants using elastomeric bearings, University at Buffalo, State University of New York 2015.

[19] Y. N. Huang, A. S. Whittaker, N. Luco, Earth. Eng. Struct. D 2010, 39(13), 1421.

[20] Y. N. Huang, A. S. Whittaker, R. P. Kennedy, et al., Earth. Eng. Struct. D 2013, 42(3), 339.

[21] H. Keikha, G. G. Amiri, J. Earthquake Eng 2019, 1 https://www.tandfonline.com/action/showCitFormats?doi=10.1080/13632469.2019.1643808

[22] M. Astrella, A. Whittaker, International workshop on performance based seismic design, At Bled, Slovenia 2004 113.

[23] Y. N. Huang, A. S. Whittaker, M. C. Constantinou, et al., Earth. Eng. Struct. D 2007, 36(12), 1741.

[24] R., Orr APP1000 Inputs for 2D SASSI Analyses, Westinghouse, 2003.

[25] R. Guide. Regulatory Guide, 2014.

[26] Guidelines for seismic performance assessment of buildings, ATC-58 50% Draft, Applied Technology Council (ATC), Redwood City, CA 2008.

[27] Y. N. Huang, S. W. Andrew, L. Nicolas, J. Stuct. Eng-ASCE 2011, 137(3), 311.